Donders' Law in Torticollis

W. P. MEDENDORP,[1] J.A.M. VAN GISBERGEN,[1] M.W.I.M. HORSTINK,[2] AND C.C.A.M. GIELEN[1]
[1]*Department of Medical Physics and Biophysics, University of Nijmegen, NL 6525 EZ Nijmegen; and* [2]*Department of Neurology, University Hospital, NL 6500 HB Nijmegen, The Netherlands*

Medendorp, W. P., J.A.M. Van Gisbergen, M.W.I.M. Horstink, and C.C.A.M. Gielen. Donders' law in torticollis. *J. Neurophysiol.* 82: 2833–2838, 1999. We investigated head movements of patients with spasmodic torticollis toward targets in various directions. These patients, whose severe dystonia was reflected in an abnormal resting head position, appeared to retain a Donders'-type strategy for the control of the rotational degrees of freedom of the head. As in normals, rotation vectors, representing head orientation, were confined to a curved surface, which specifies how head torsion depends on gaze direction. The orientation of the surface in body coordinates, which was very stereotyped in normals, was different for patients. The same Donders surface was found for head movements and for stationary head postures, indicating that the same neural mechanism governs its implementation in both tasks. To interpret our results, we propose a conceptual scheme incorporating the basal ganglia, which are thought to be involved in the etiology of torticollis, and an implementation stage for Donders' law.

INTRODUCTION

Natural head postures are the result of movements of the head relative to the upper vertebrae and of movements of the neck vertebrae. This biomechanical system has three rotational degrees of freedom, which is obvious from the fact that subjects can voluntarily rotate the head about any axis in three-dimensional (3-D) space. A particularly suitable method for describing orientations of systems with three rotational degrees of freedom, like the head, is by means of rotation vectors (Haustein 1989). During natural gaze shifts, the actual repertoire of head orientations appears to be constrained to rotation vectors in a two-dimensional (2-D) surface (Glenn and Vilis 1992; Medendorp et al. 1998; Radau et al. 1994). This result reflects a reduction of the number of degrees of freedom, known as Donders' law. Up until now, it is not clear where in the neural pathways involved in head movement control Donders' law is implemented. In a recent model, Tweed (1997) proposed that Donders' law for the head is implemented neurally downstream of the superior colliculus. In the present paper we explore what may be learned about these neural mechanisms by studying the control of head positions in a group of patients with spasmodic torticollis. Spasmodic torticollis is a focal dystonia characterized by abnormal movements and postures of the head and the neck. The origin of this pathology is thought to reflect a disorder of the basal ganglia (Berardelli et al. 1998). The aim of this study is to investigate whether patients with spasmodic torticollis demonstrate a Donders'-type strategy and, if so, whether the corresponding 2-D surface with head rotation vectors is the same as in normals.

The costs of publication of this article were defrayed in part by the payment of page charges. The article must therefore be hereby marked "*advertisement*" in accordance with 18 U.S.C. Section 1734 solely to indicate this fact.

METHODS

Subjects

In this study we tested five normal subjects (age 46–58 yr.) and 5 patients with idiopathic spasmodic torticollis (age 54–75 yr, no medication). All patients had a moderate to severe head deviation, as indicated by their resting position in Fig. 1.

Experimental approach

Subjects were tested while seated and were restrained to minimize movements of the trunk. In the Movement paradigm, they were asked to make gaze shifts toward 12 equi-eccentric (40°) targets (verbally indicated) in different directions arranged along a circular array in the frontal plane, like the hours on the face of a clock, starting from the center of the circle. As shown in Fig. 1, head movements typically did not reach 40° eccentricity, especially not in the patient group. Each eccentric target was tested three times, and each trial lasted for ~4 s. In the Fixation paradigm the subject was asked to move from the resting position to one of the 12 eccentric targets and to maintain peripheral fixation for ~10 s. During the experiment, head position in 3-D was recorded using an OPTOTRAK 3020 system. The subject wore a helmet-mounted array of eight infrared-light-emitting diodes (ireds), which could be tracked by the OPTOTRAK system. The coordinates of the ireds were transformed to a right-handed body-fixed coordinate system whose *x*-*y* plane was aligned with the subject's transversal plane (*x*-axis pointing forward, *y*-axis leftward, *z*-axis upward). The position of the helmet on the head was calibrated with respect to the ear canals and the eyes (see Medendorp et al. 1998, for further details). We also measured the resting position of the head, instructing the patient to accept his abnormal head posture. All data were collected using a sample frequency of 100 Hz.

Description of head positions using a virtual reference position

All head positions were determined with respect to a virtual reference position that was based on the mean position of anatomic landmarks (i.e., ear canals and eyes) of normal subjects keeping their head erect and their eyes horizontally looking at infinity. For this head position, Jampel and Shi (1992) found that the mean angle between the visual line and the cantomeathal line (i.e., the line from the center of the interaural axis to the cyclopean eye) is 15°. Because of their disease, most patients were physically incapable to adopt a normal upright head position. Therefore, for each subject, we computed from the calibration data the head orientation for which the cantomeathal vector is at an angle of 15° with the straight-ahead direction (the *x*-axis) and for which the interaural axis is aligned with the *y*-axis of the body-fixed coordinate system. In this way, by using a common reference position for normals and patients, we ensured that head position data could be compared directly. Calibration errors in the virtual reference position were ≤3°.

Any instantaneous head position was then described as the result of a virtual rotation from the fixed virtual reference position to the

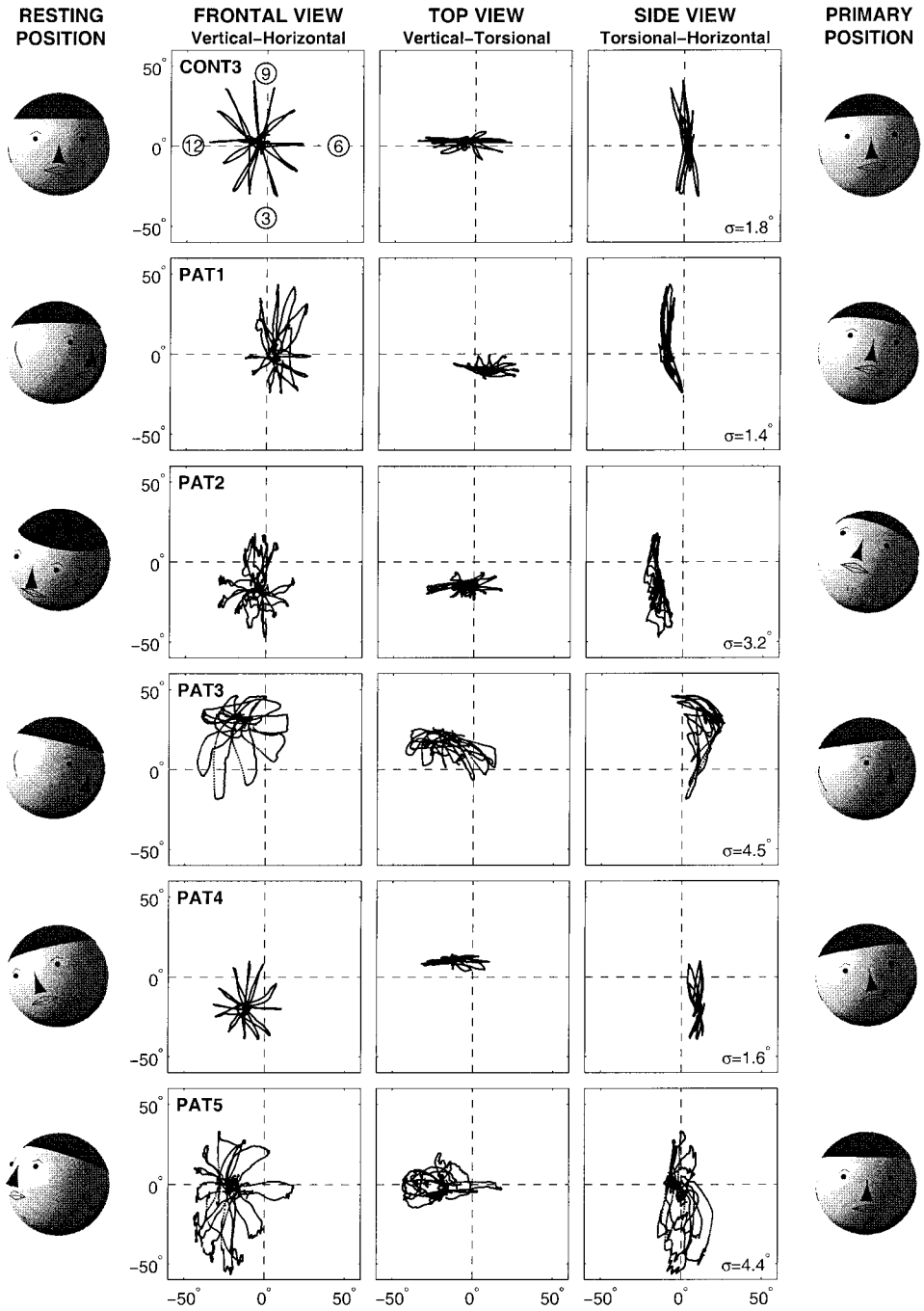

FIG. 1. Head rotation vectors from a representative control subject (*top row*) and all patients. Frontal, top, and side views contain 1 to-and-fro movement in each direction. Target directions 3, 6, 9, and 12 o'clock are indicated in the *top* frontal view panel. Axes are calibrated in degrees. In the *left-hand column* the resting position of the head is shown as calculated from the anatomic landmarks (see METHODS). The primary head positions, depicted in the *right-hand column*, show clear deviations from the erect head position in most patients. The thickness values of the fitted surface (σ in degrees), denoted in the side-view panels, demonstrate that both controls and patients keep the torsional components limited.

current position. The corresponding rotation vector is given by $\vec{r} = \tan(\theta/2) \cdot \vec{n}$, where $\vec{n}$ represents the direction of the rotation axis and $\tan(\theta/2)$ is the amount of rotation by an angle θ about that axis (Haustein 1989).

Data analysis

Onset and offset of center-to-target and target-to-center movements were determined on the basis of an angular velocity criterion (<5°/s). To check how well a curved surface can describe the data, we fitted a second-order function, given by $r_x = a + br_y + cr_z + dr_z^2 + er_yr_z + fr_z^2$ to the rotation vectors in which r_x, r_y, and r_z represent the torsional, vertical, and horizontal components, respectively. The scatter of the data relative to the fitted surface (thickness) is defined by the standard deviation of the distances of all samples in the r_x-direction to the fitted surface (in degrees).

To characterize its orientation, we approximated the surface as a flat plane, thus ignoring the second-order terms. Note that this plane, given by $r_x = a + br_y + cr_z$, may be shifted relative to the origin of the coordinate system (i.e., $a \neq 0$) because all measured head orientations may have a torsional displacement relative to the virtual reference position. From the flat plane fit, we obtained the rotation vector $\vec{P}$, which rotates the anatomically defined reference position into the primary position, using $\vec{P} = (a, c, -b)^T$ (for derivation, see Haustein 1989). Conceptually, characterizing each subject by his primary head position provides direct insight in the adopted head orientation in any other gaze direction because each position can be conceived as the result of rotating the head from the primary position by an axis perpendicular to the primary direction. Equivalently, differences among subjects concerning the plane of rotation vectors are fully reflected in different primary head positions. This is only an

approximation in the sense that the notion of a primary position is only strictly valid for a flat plane.

RESULTS

The *three middle columns* in Fig. 1 show the head movements from the center toward each of the 12 eccentric targets for 1 typical control subject (*CONT3*) and for the 5 patients, whose resting position is shown on the *left*. The frontal view column shows the horizontal and vertical components of the rotation vectors in body coordinates. For the patients, the frontal view panels demonstrate that the movement trajectories generally show a more jerky and irregular pattern. The top view column and the side view column show the torsional components as a function of the vertical and horizontal component, respectively. Both the control subjects and the patients keep their torsional components restricted to a rather small range for all movement directions. Furthermore, the torsional components of *patients 1–4* are shifted with respect to the origin (see top view and side view columns).

We fitted a second-order surface to the head rotation vectors, to check how well a curved surface could describe the data from each subject. The parameters of the fitted surface are presented in Table 1. In the controls, the thickness of these surfaces varied between 0.8 and 1.8° and was on average 1.2 ± 0.4° (mean ± SD), indicating small torsion deviations from the fitted surface. For the patients, the thickness ranged from 1.4 to 4.5° (see σ-value in 4th column), which remains small, given movements of ~30°. In three patients (*2*, *3*, and *5*), the difference with the controls was significant (*t*-test; $P < 0.05$). Regarding the shape of the surface of the control subjects, the only significant second-order term was the twist score, represented by parameter *e*, which was on average −0.84 ± 0.23. On average, the coefficients *b* and *c* were not significantly different from zero ($P < 0.05$), indicating that the average surface of the controls is aligned with the *yz*-plane of the coordinate system, as reported before (Medendorp et al. 1998). For the patients, we found more intersubject variability in the curvature of the surfaces, as shown in Table 1. For a better understanding of these fit parameters, we have depicted the head orientations that correspond to the curved-surface fit in Fig. 2*A*.

We fitted a flat plane to the rotation vector data to determine the rotation vector $\vec{P}$ (see METHODS) that rotates the reference position into the primary position for each subject. The corresponding primary head positions are depicted in the right-hand column of Fig. 1. For normal subjects, the primary position is close to the normal erect position. Deviations from the normal erect position remained within 3° in the torsional direction, within 2° from the mid-sagittal plane, and ranged up to 6° from the horizontal plane. On average, the rotation vector $\vec{P}$ of the controls is not significantly different from a zero rotation vector (*t*-test, $P > 0.3$), which means that the average surface is virtually aligned with the *yz*-plane of the coordinate system. The primary head position for each patient (except for *PAT5*) shows clear deviations from the normal erect position. Deviations range up to 17° in torsional direction (for *PAT2*), up to 26° from the mid-sagittal plane (for *PAT3*) and up to 20° from the horizontal plane (for *PAT2*). When at least one of the coefficients characterizing the rotation vector $\vec{P}$ of a patient deviates by more than 2 SDs from the mean rotation vector $\vec{P}$ of the control subjects, we regard the corresponding primary position as significantly different. On this basis, the primary head positions of *patients 1–4* are abnormal.

Finally, we tested whether a second-order surface can describe the head orientations as accurately during fixations (using the fixation paradigm) as during the movements. As shown in Fig. 2*B*, all patients (except *PAT 4*) show a rather poor fixation behavior. The numbers in the figure specify the size of each ellipse in torsional direction. There are considerable differences in how strictly Donders' law is obeyed, but when a Donders surface was computed from the total set of fixation data of each patient, its thickness was comparable with that derived from the movement data (see *2 most right-hand columns* in Table 1). Statistically, both the control group and the patient group revealed no differences between the orientation and SDs of the fits to the movement data and to the data during

TABLE 1. *Results of a second-order surface fit to the movement data for each subject*

	Movement							Fixation
Subject	*a*	*b*	*c*	*d*	*e*	*f*	σ, deg	σ, deg
C1	0.025 ± 0.001	−0.078 ± 0.002	−0.018 ± 0.001	0.367 ± 0.016	−0.853 ± 0.012	0.027 ± 0.004	0.8	0.7
C2	−0.021 ± 0.001	0.003 ± 0.002	0.162 ± 0.001	0.103 ± 0.012	−0.928 ± 0.009	−0.141 ± 0.004	1.2	1.3
C3	0.023 ± 0.001	0.015 ± 0.002	−0.115 ± 0.001	−0.013 ± 0.009	−1.053 ± 0.010	−0.183 ± 0.006	1.8	1.9
C4	0.022 ± 0.001	−0.051 ± 0.001	0.009 ± 0.001	0.004 ± 0.006	−0.898 ± 0.007	−0.121 ± 0.004	0.8	0.9
C5	−0.034 ± 0.001	0.013 ± 0.002	−0.012 ± 0.001	0.019 ± 0.007	−0.442 ± 0.007	0.033 ± 0.004	1.2	0.9
Mean	0.003 ± 0.028	−0.020 ± 0.042	0.005 ± 0.100	0.096 ± 0.158	−0.835 ± 0.232	−0.077 ± 0.100	1.2	1.1
P1	−0.085 ± 0.001	−0.152 ± 0.002	−0.167 ± 0.001	0.655 ± 0.012	−0.643 ± 0.009	0.717 ± 0.004	1.4	1.1
P2	−0.169 ± 0.001	−0.064 ± 0.006	−0.194 ± 0.005	−0.090 ± 0.022	−0.987 ± 0.029	0.106 ± 0.014	3.2	2.7
P3	0.088 ± 0.002	−0.220 ± 0.014	0.377 ± 0.011	−0.376 ± 0.030	−0.547 ± 0.033	−1.532 ± 0.023	4.5	5.0
P4	0.061 ± 0.001	−0.316 ± 0.003	−0.224 ± 0.002	−0.333 ± 0.010	−1.596 ± 0.012	−0.310 ± 0.006	1.6	1.7
P5	−0.015 ± 0.001	−0.056 ± 0.007	−0.193 ± 0.005	0.011 ± 0.019	−1.172 ± 0.022	0.071 ± 0.010	4.4	5.1

Values are means ± SD. Rotation vector data of both control subjects (C) and patients (P) were fitted using the equation $r_x = a + br_y + cr_z + dr_y^2 + er_yr_z + fr_z^2$. The parameters are expressed in body coordinates. The SD of the distance of the rotation vectors in the r_x-direction to the fitted surface is given by σ (in degrees). Note that on average the largest second-order term for the controls is the twist score $e = -0.835$. The fact that the coefficients *b* and *c*, characterizing the orientation of the plane, are near zero for the control subjects indicates that the plane is nearly aligned with the *yz*-plane of our coordinate system. This is not the case for the patient group. Further, the coefficients *d*, *e*, and *f*, describing the curvature of the surface, show more intersubject variability for patients than for the control subjects. The *right-hand column* shows the thickness of the second-order fit to the fixation data of each subject, indicating no differences in comparison with the fit to the movement data (parameter σ in adjacent column).

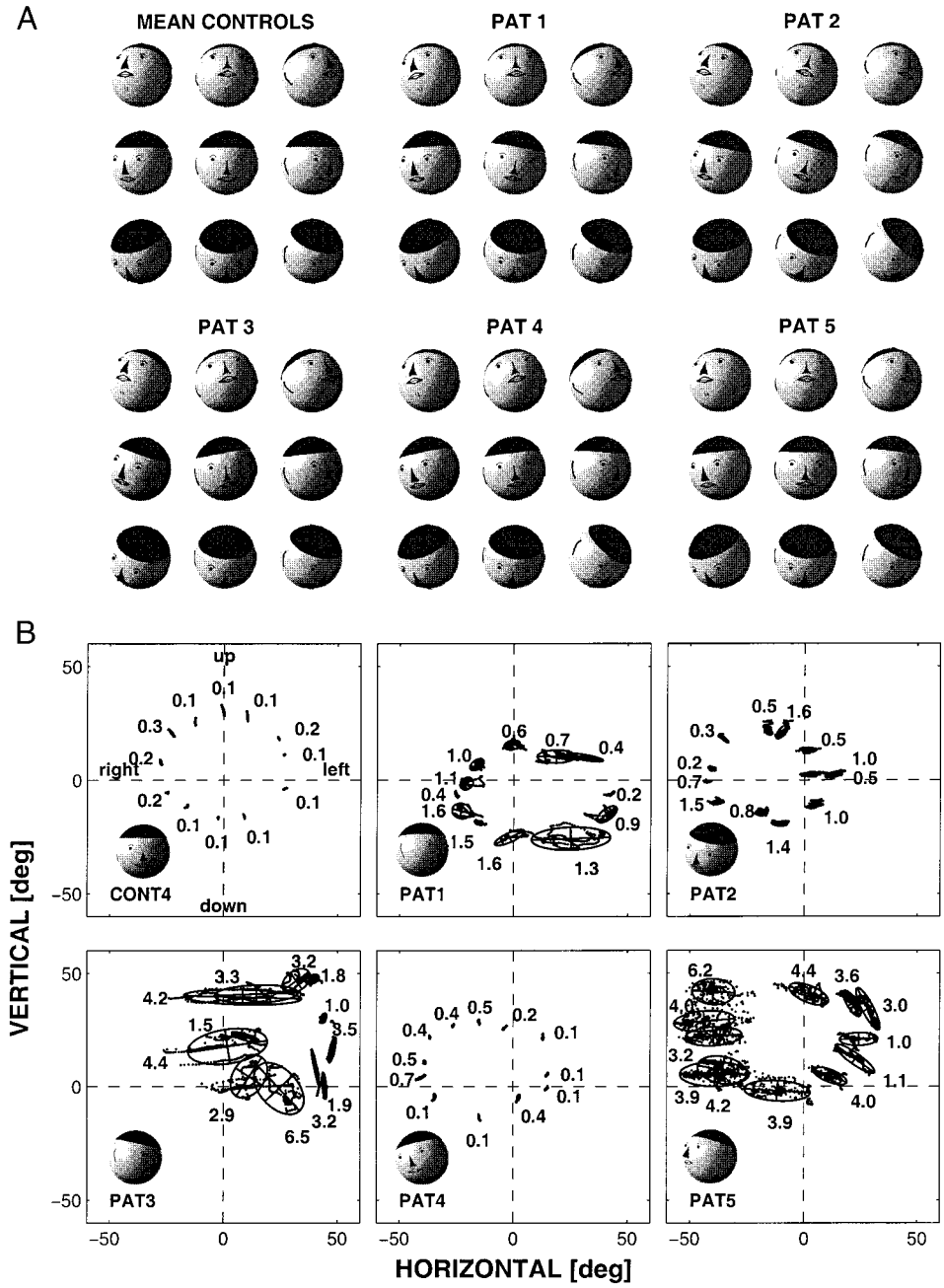

FIG. 2. *A*: 9 head orientations representing the best curved-surface fit. The head postures in vertical or horizontal directions are shown for −30, 0, or 30°. Figure shows vividly that there are differences between each patient (except *patient 5*) and the mean head orientations of the controls. Note that because the fit was determined using the data in the restricted movement range of the patients (see Fig. 1), some of the depicted head orientations were not really adopted by the patients but are interpolated on the basis of the fit parameters. *B*: fixation performance of one control subject (*CONT4*) and all patients. Each panel shows head fixations to each eccentric target by plotting the horizontal and vertical components in degrees for a single 10-s recording. For clarity, each panel also shows the resting position of the head. Further, ellipses have been fitted to the data to characterize the variations in head position while fixating each target. Next to the ellipses, their size in torsional direction is given in degrees. Control *subject 4*, shown here, is representative for all controls. *Patient 4* shows a reasonably good fixation control, similar to normal subjects, but the other patients range from minor difficulties (*PAT2*) to a very poor fixation control (*PAT1, 3,* and *5*). With regard to the movement range in different directions, the center of the ellipse array is shifted in the direction of the resting position so that movement excursions to targets opposite to the resting position are relatively small. There is no clear-cut relation between the preferred head orientation in rest and the direction with the largest scatter during fixation.

the fixation period [controls: ANOVA $F(1,4) = 0.06$; $P > 0.05$, and patients: $F(1,4) = 0.19$; $P > 0.05$].

Closer inspection of Fig. 2*B* suggests that the torsional thickness of the fixation clusters in some patients is not uniform but depends on target direction. To explore whether there is a general tendency that larger clusters in the horizontal-vertical plane are thicker in torsional direction, the data of each patient were analyzed in more detail. We found a significant relation between the size of the ellipse and the torsional thickness for one patient only (*patient 3*: $r = 0.63$, $P < 0.05$, $n = 12$). The data from normal subjects were similar to those of control *subject 4* in Fig. 2*B* in showing very small scatter values in both horizontal and vertical direction and in torsion, without any clear hint of target dependence. As Table 1 shows, the fixation data of the normal subjects yielded a Donders surface that was just as thin as that computed from the movement data.

DISCUSSION

The present study has yielded two striking findings. On the one hand, violations of Donders' law were surprisingly modest (σ range: 1.4–4.5°), even in patients with the most severe torticollis symptoms. On the other hand, the fact that most patients had abnormal primary positions (see Fig. 1), reflecting abnormally oriented or shifted fit surfaces (Fig. 2*A*), indicates that they handle the reduction in rotational degrees of freedom differently. These deviations support the hypothesis that the

reduction is at least partly due to neurally imposed constraints, in agreement with suggestions in a recent study of Crawford et al. (1999). Moreover, the fact that we found virtually no differences in the control of degrees of freedom in postural tasks and movement tasks suggests that the same neural mechanism is involved in head position control in both tasks.

If we are to understand these findings, in principle, it is necessary to have a specific model of where Donders' law is implemented as part of a larger scheme that identifies the dysfunctional neural areas and specifies how they cause the torticollis. Probably because the present study has been the first of its kind, such a complete scheme is not available. The relevant models that have been proposed to deal with these issues are limited to just one aspect (either to Donders' law or to torticollis neuropathology). To make a first step, we will now explore how these separate models can be merged, to see how a unified scheme can make sense of our results (Fig. 3).

There is general agreement that the superior colliculus (SC) is heavily involved in visually guided gaze shifts (Freedman and Sparks 1997; Guitton 1992) and that its signals, coding gaze error, are 2-D in nature (Hepp et al. 1993; Van Opstal et al. 1991). For a correct gaze shift, this 2-D gaze error signal must be converted into appropriate 3-D head and eye rotations. A recent model of eye-head saccades by Tweed (1997) suggests that the 2-D gaze error signal passes through a Donders operator to specify the correct 3-D head position signal. For the eye, the 2-D gaze error signal and the 3-D head position signal pass through a Listing operator to yield a 3-D eye position signal that fits Listing's law for eye in head. In other words, both operators are located downstream from the SC. Unfortunately, Tweed's scheme assigns no role to the basal ganglia (BG), which are thought to play a key role in torticollis.

The combined conceptual scheme in Fig. 3 immediately raises an interesting problem. If the BG are responsible for the abnormal head resting posture seen in the patients, the question arises how and where their aberrant signals are affecting the gaze control system. Clinical studies suggest that the dystonia results from a functional disturbance of the basal ganglia. This would lead to an abnormal regulation of brain stem and spinal cord inhibitory interneural mechanisms (see Berardelli et al. 1998 for review), resulting in a constant activation of some neck muscles. In line with this, we propose in the scheme (see *option 1*) that a disturbed BG signal affects the gaze control system at a peripheral level downstream of the Donders operator by causing a bias signal on the motoneurons. This bias signal causes an additional head position signal to the motoneurons, responsible for the abnormal resting position of torticollis patients. The signal from the pulse-step generator (PSG) consists of a velocity and a position component. In the scheme, we hypothesize that the bias signal and PSG signal converge at the motoneuron level. Figure 3*B* shows the predictions of the model for several expressions of the BG signal. One effect of the BG vector is to induce an abnormal resting position of the head, reflecting its direction and amplitude. To overcome this bias in targeting movements, compensatory commands through the SC have to be generated. The simulations were made to illustrate qualitatively that the same bias signal may be responsible for certain imperfections in the implementation of Donders' law. For simplicity, the assumption was made that the Donders operator encodes a flat Donders surface (see *left-hand panels*). We first consider the

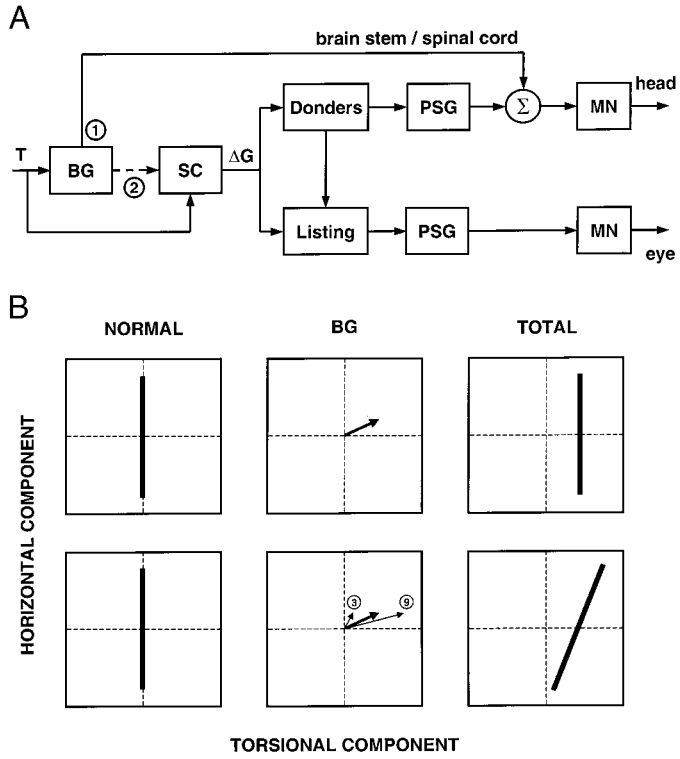

FIG. 3. Conceptual scheme for head position control in torticollis patients. To foveate a new point of interest (*T*), a redirection of gaze is required. This desired gaze displacement (ΔG) is coded by the superior colliculus (SC) as a two-dimensional (2-D) gaze error signal. The 2-D gaze signal passes through a Donders operator to yield a three-dimensional (3-D) head position signal that obeys Donders' law (unless voluntarily overridden). The 2-D gaze signal and 3-D head position signal pass through a Listing operator to yield the correct 3-D eye position signal, obeying Listing's law. Both signals then travel through a pulse-step generator (PSG), in which they are converted to position and velocity signals to drive the head and eye motoneuron pool (MN). *B*: predictions of the model for *option 1*, which proposes that the basal ganglia (BG) affect the gaze control system at a peripheral level downstream of the Donders operator by causing a bias signal on the motoneurons. The model proposes that the Donders box, by itself, encodes a normal Donders surface (see *left-hand panel*) and that all abnormalities in the actual surface of the patients (*right-hand column*) reflect effects of the BG signal (*middle column*). When the BG signal is constant, as shown by the BG vector in the *top panel*, the Donders surface would only be affected by its torsional component. This will then lead to a shift of the plane with rotation vectors, but not to a violation of Donders' law. In case the BG bias signal is not constant, but varies in 3-D (see the shaded area around the BG vector), the Donders surface will become thicker (*right-hand panel*). For a BG signal with a target-dependent torsional component (see *bottom panel*, which shows a BG signal that differs from the default value for a 3 and a 9 o'clock target), the model predicts both a shift and a tilt of the rotation vector surface. On the basis of *option 2* in the scheme, where abnormal BG signals affect the system at a level upstream of the Donders operator, no abnormalities in Donders surface would be expected.

simple case that the BG signal is constant, as shown by the BG vector in the *top middle panel.* The Donders surface will only be affected if the BG vector has a torsional component. Such a torsional BG component will cause a shift of the plane containing the rotation vectors, but not a violation of Donders' law. The torsional shift in the primary head position of some patients (see Fig. 1) can be understood in this fashion. The data from several patients indicate that the dystonia may fluctuate in time (Fig. 2*B*). When the BG signal varies in 3-D, as indicated by the gray patch surrounding the BG vector, the Donders surface will become thicker (as observed in *patients 3* and *5*). Finally, in the more complex case that the BG signal has a

target-dependent torsional component (see *bottom row*), the model yields both a shift and a tilt of the rotation vector surface, but again no violation of Donders' law as such. Of course, if the BG signal has a less regular dependence on target position, an abnormally curved Donders surface may be created. By making assumptions about target-dependent variations of the BG signal (reflected by the size and the shape of the gray patch), one might be able to account for the differences in 3-D fixation behavior at different target locations (see Fig. 2*B*), but we feel that this would stretch the scheme too far.

The second possibility in Fig. 3 (*option 2*), that the BG signal may affect movements by the connection to the SC, studied by Hikosaka and Wurtz (1983), does not provide a simple explanation of the posture problems in the patients because the SC codes displacements, not postures. If this pathway were nevertheless involved, its signal would not spoil the maintenance of Donders' law, which is implemented more downstream.

A recent study of 3-D eye movement control in strabismus has provided an interesting analogy (Melis et al. 1997). These authors found that a strabismus patient, where a similar peripheral bias problem may be assumed to occur, nevertheless had clear Listing planes, but with different orientations in the two eyes.

A limitation of the present study is that it has been restricted to head movements. Because eye and head have to cooperate closely in eye-head saccades (Tweed et al. 1995), it would be very interesting to investigate, in future work, how this cooperation works out in 3-D. Will the eye compensate for abnormalities in the orientation and the curvature in Donders surface? If these abnormalities reflect abnormal BG signals operating at a peripheral level (*option 1* in Fig. 3) as we have suggested, the model implies that the Listing box in the model will not be informed about the resulting deficiencies so that the final 3-D gaze direction will be affected as well. We conclude that further quantitative studies of the gaze control system in these patients are promising for a better understanding of the neuropathology and as a test for models of gaze control.

Address for reprint requests: W. P. Medendorp, Dept. of Medical Physics and Biophysics, University of Nijmegen, Geert Grooteplein 21, NL 6525 EZ Nijmegen, The Netherlands.

Received 16 February 1999; accepted in final form 4 June 1999.

REFERENCES

BERARDELLI, A., ROTHWELL, J. C., HALLETT, M., THOMPSON, P. D., MANFREDI, M., AND MARSDEN, C. D. The pathophysiology of primary dystonia. *Brain* 121: 1195–1212, 1998.

CRAWFORD, J. D., CEYLAN, M. Z., KLIER, E. M., AND GUITTON, D. Three-dimensional eye-head coordination during gaze saccades in the primate. *J. Neurophysiol.* 81: 1760–1782, 1999.

FREEDMAN, E. G. AND SPARKS, D. L. Activity of cells in the deeper layers of the superior colliculus of the rhesus monkey: evidence for a gaze displacement command. *J. Neurophysiol.* 78: 1669–1690, 1997.

GLENN, B. AND VILIS, T. Violations of Listing's law after large eye and head gaze shifts. *J. Neurophysiol.* 68: 309–318, 1992.

GUITTON, D. Control of eye-head coordination during orientating gaze shifts. *Trends Neurosci.* 15: 174–179, 1992.

HAUSTEIN, W. Considerations of Listing's law and the primary position by means of a matrix description of eye position control. *Biol. Cybern.* 60: 411–420, 1989.

HEPP, K., VAN OPSTAL, A. J., STRAUMANN, D., HESS, B.J.M., AND HENN, V. Monkey superior colliculus represents rapid eye movements in a two-dimensional motor map. *J. Neurophysiol.* 69: 965–979, 1993.

HIKOSAKA, O. AND WURTZ, R. H. Visual and oculomotor functions of monkey substantia nigra pars reticulata. IV. Relation of substantia nigra to superior colliculus. *J. Neurophysiol.* 49: 1285–1301, 1983.

JAMPEL, R. S. AND SHI, D. X. The primary position of the eyes, the resetting saccade, and transverse visual head plane. *Invest. Ophthalmol. Vis. Sci.* 33: 2501–2510, 1992.

MEDENDORP, W. P., MELIS, B.J.M., GIELEN, C.C.A.M., AND VAN GISBERGEN, J.A.M. Off-centric rotation axes in natural head movements: implications for vestibular reafference and kinematic redundancy. *J. Neurophysiol.* 79: 2025–2039, 1998.

MELIS, B.J.M., CRUYSBERG, J.R.M., AND VAN GISBERGEN, J.A.M. Listing's plane dependence on alternating fixation in a strabismus patient. *Vision Res.* 37: 1355–1366, 1997.

RADAU, P., TWEED, D., AND VILIS, T. Three-dimensional eye, head, and chest orientations after large gaze shifts and the underlying neural strategies. *J. Neurophysiol.* 72: 2840–2852, 1994.

TWEED, D. Three-dimensional model of the human eye-head saccadic system. *J. Neurophysiol.* 77: 654–666, 1997.

TWEED, D., GLENN, B., AND VILIS, T. Eye-head coordination during large gaze shifts. *J. Neurophysiol.* 73: 766–779, 1995.

VAN OPSTAL, A. J., HEPP, K., HESS, B.J.M., STRAUMANN, D., AND HENN, V. Two- rather than three-dimensional representation of saccades in monkey superior colliculus. *Science* 252: 1313–1315, 1991.